Birefringence of a Polystyrene Solution in Elongational Flow: Effects of Molecular Weight and Solvent Quality

Tuan Q. Nguyen,* Guozhu Yu, and Henning-H. Kausch

Department of Materials Science, Polymer Laboratory, Swiss Federal Institute of Technology, MX-D, CH-1015 Lausanne, Switzerland

Received June 17, 1994; Revised Manuscript Received March 13, 1995®

ABSTRACT: Elongational flow was created by forcing dilute PS solutions across two jets in exact opposition. The retardation signal was mapped across the birefringence domain as a function of fluid strain rate, polymer concentration, MW, and solvent quality. The use of a fast polarization-modulation technique in conjunction with signal averaging increased the detection limit by over 1 order of magnitude in comparison to static-polarization experiments. Retardation could be determined at polymer concentrations down to the ppm level. The critical strain rate ($\dot{\epsilon}_c$) for molecular coil orientation was corrected for polymer dispersity by combining the birefringence curves with the MWD obtained by gel permeation chromatography. In contrast with previous investigations, it was found that $\dot{\epsilon}_c$ depended on the solvent quality and scaled with polymer molecular weight (M) as $\sim M^{-1.5}$ in a poor solvent (decalin) and as $\sim M^{-1.8}$ in good solvents (toluene and 1-methylnaphthalene). The possibility of using flow birefringence to determine polymer molecular weight distribution has been assessed and compared to the more conventional technique of gel permeation chromatography. The large dispersion in the birefringence curves suggested a gradual increase in segmental orientation with the fluid strain rate instead of an abrupt coil-to-stretch transition.

Introduction

In the late 1970s, Pope and Keller observed a highly localized birefringence zone when dilute polymer solutions were pumped across two narrow orifices in exact opposition.[1] The birefringence was visible only above a critical value of the fluid strain rate ($\dot{\epsilon}_c$) which was on the order of the reciprocal chain relaxation time (τ_1)

$$\dot{\epsilon}_c = B/\tau_1 \quad \text{with } B \sim 1 \tag{1}$$

From the strain-rate dependence and the amplitude of the birefringence signal, it was concluded[1] that the chains became highly extended above the critical strain rate $\dot{\epsilon}_c$, in accordance with the abrupt coil-to-stretch transition predicted by de Gennes.[2]

However, a few points remain unresolved within this seemingly coherent picture. There is no general agreement about the exact value for the factor B in eq 1. Part of this discrepancy may be traced back to the different models used to derive eq 1 and to the diverse numerical expressions for τ_1. For a Hookean dumbbell, unbound expansion in steady elongational flow is predicted at $\dot{\epsilon}_c = 0.5/\tau_H$ (τ_H = dumbbell relaxation time).[3] More elaborate calculations based on the bead–spring model with hydrodynamic interactions give $B = 0.5035$, which is just 7% above the value for the Hookean dumbbell.[4,5] Higher estimations for B are, however, frequently found in the literature, with 1 being the most cited value.[6]

For a non-free-draining chain, the longest relaxation time is usually related to the unperturbed root-mean-square end-to-end distance R through the relation:[7]

$$\tau_1 = 0.398R^3\eta_s/k_BT \tag{2}$$

where η_s is the solvent viscosity, k_B the Boltzmann constant, and T the absolute temperature.

For eq 1 to be valid, $\dot{\epsilon}_c$ should scale with polymer MW as $1/R^3$, i.e.

$$\dot{\epsilon}_c \sim 1/\tau_1 \sim M^{-3\nu} \tag{3}$$

In this equation, ν is a coefficient equal to 0.50 in a Θ-solvent and 0.59 in a good solvent.[8]

In a detailed series of investigations, Keller and Odell[9,10] established that the dependence of $\dot{\epsilon}_c$ on $M^{-1.5}$ is universal, regardless of the solvent quality. This result implies that the parameter B is not constant but increases with polymer molecular weight as $\sim M^{0.3}$ in a good solvent. It was suggested that this "anomaly" may be rationalized if the molecular relaxation time and the critical strain rate obey different scaling laws.[11] Using a Flory's type mean-field approach, Rabin derived the following relation for the critical strain-rate instead of eq 3:[11,12]

$$\dot{\epsilon}_c \sim 1/\tau_1 \sim M^{-(1+\nu)} \tag{4}$$

The exponent range of −1.5 to −1.6 predicted by eq 4 was in better agreement with the precedently reported experimental results.[9,10]

The birefringence equipments used in previous investigations were of the static-type based on the Senarmont compensator. In recent years, several improvements have been made which allow significant gain in sensitivity and in acquisition time. The class of polarimeters that has been most extensively investigated relies on the modulation of light polarization. In the present paper, a version of the rotary modulation technique developed by Fuller[13] and commercialized by Rheometrics U.S. (Rheometrics Optical Analyzer or ROA) was used for the measurements.

The present work is intended to be purely experimental with a 3-fold purpose: first, to test the gain in sensitivity attainable with the new generation of polarization-modulated instruments under dynamic conditions of flow; second, to investigate in a more quantitative way the relationship between the critical strain rate for birefringence and the chain relaxation time, after due consideration of sample polydispersity; third, to check for the feasibility of using flow birefringence as a reliable method of molecular weight characteriza-

* To whom correspondence should be addressed.

® Abstract published in *Advance ACS Abstracts,* June 15, 1995.

0024-9297/95/2228-4851$09.00/0

tion in comparison with more conventional techniques such as gel permeation chromatography.

Experimental Section

Chemicals. The polystyrene samples were narrow molecular weight standards from Polymer Laboratories (Shropshire, U.K.) with M_p (MW at peak maximum) in the range of $1.46 \times 10^6 - 20 \times 10^6$. The polydispersity index, $\bar{M}_w/\bar{M}_n$, was <1.05 for molecular weights below 4×10^6 and up to 1.20 for the highest molecular weight samples.

The solvents, from Fluka AG (Switzerland), were purified by distillation prior to the experiments. Decalin is a mixture of 58% *trans*- and 41% *cis*-decahydronaphthalene + 1% tetrahydronaphthalene as determined by gas chromatography. The experimental Θ-temperature for PS in decalin is 14.8 °C.[14] The polymer solutions are gently stirred for 24 h and then passed through a 14-μm sintered-glass filter prior to experiments.

Intrinsic Viscosity of Polystyrene Solutions. Two alternative techniques, depending on the polymer MW, have been employed for the determination of the intrinsic viscosity. This experimental procedure was dictated by the following considerations: it is well-known that dilute polymer solutions are shear-thinning in capillary flow above a wall shear rate $\dot{\gamma} \sim 1/\tau_1$. For high-MW polymers, it is necessary to conduct experiments at very low shear rate to avoid viscoelastic corrections. In addition, according to our experience, the MW averages quoted by the vendors are only approximate in the ultrahigh-MW range. For example, a PS sample commercialized as a 14.4×10^6 standard has in reality a M_p of 21×10^6, a $\bar{M}_v$ of 18×10^6, and $\bar{M}_w = 15 \times 10^6$ as determined by GPC, viscometry and low-angle laser light scattering, respectively.

The kinematic viscosity of PS solutions with MW $\leq 3 \times 10^6$ was measured with an automatic Ubbelohde viscometer (Schott AVS-310). After correction for the solvent density (ϱ_s), the following Mark–Houwink–Sakurada (MHS) relationships have been obtained at 295 K which was also the experimental temperature:

PS/decalin

$$\eta_s = 2.39 \text{ mPa·s}$$

$$[\eta] = 2.34 \times 10^{-3} M^{0.53} \text{ m}^3\text{·kg}^{-1}$$

$$\varrho_s = 879.8 \text{ kg·m}^{-3} \quad (5)$$

PS/toluene

$$\eta_s = 0.585 \text{ mPa·s}$$

$$[\eta] = 1.58 \times 10^{-3} M^{0.71} \text{ m}^3\text{·kg}^{-1}$$

$$\varrho_s = 863.1 \text{ kg·m}^{-3} \quad (6)$$

PS/1-methylnaphthalene

$$\eta_s = 3.02 \text{ mPa·s}$$

$$[\eta] = 1.87 \times 10^{-3} M^{0.70} \text{ m}^3\text{·kg}^{-1}$$

$$\varrho_s = 1020 \text{ kg·m}^{-3} \quad (7)$$

(η_s, solvent viscosity, $[\eta]$, intrinsic viscosity; in the above equations, the polymer molecular weight (M) is given in units of kg·mol^{-1}).

In the MW range $>3 \times 10^6$, the viscosity detector of the Waters 150CV was used for intrinsic viscosity determination. The standard capillary was replaced with 100 cm stainless steel tubing of 0.1 cm internal diameter. By measuring the viscosity of a 19×10^6 PS solution as a function of flow rate, it was shown that shear thinning was negligible for flow rates ≤0.50 mL/min (which correspond to wall shear rates ≤80 s^{-1}). With the appropriate MHS coefficients and the GPC data, it was verified that the MWs given by the manufacturer were generally accurate to within ±10%. Exceptions were the previously mentioned, "14.4×10^6", polymer and a "20×10^6" standard which had a correct $M_p = 19 \times 10^6$ but a $\bar{M}_v = 15 \times 10^6$ and a $\bar{M}_w = 14 \times 10^6$ well below the sample specifications.

Molecular Weight Distribution. The molecular weight distribution was determined by gel permeation chromatography (GPC) on a Waters 150CV, equipped with special columns for ultrahigh-MW polymers (TSK G7000HXL and Ultrastyragel 10^6 Å) and diode-array detection (Kontron Model DAD-440). A PC-compatible personal computer was used for data acquisition and analysis. Polymers with MW above 3×10^6 are particularly prone to mechanochemical degradation. To preserve polymer integrity, extreme care should be exercised during the preparation, injection, and analysis of the samples. Experimental conditions for a successful GPC characterization in the ultrahigh-MW range have been described earlier.[15]

Elongational Flow. The experimental setup employed for the creation of stagnant elongational flow is shown schematically in Figure 1. In the design of the opposed jets cell, interchangeable nozzles were used with a gap distance continuously adjustable with a rotary screw. The jet tips were made of synthetic sapphire with a precisely bored circular orifice connected to a 60° tapered channel. The susceptibility of high-MW polymers to shear-induced degradation imposed severe restrictions on the choice of the pumping system which, in addition, must deliver a constant and pulseless flow rate. After several trials, a 500-mL syringe pump capable of transferring up to 205 mL/min of polymer solution (ISCO Model 500D) was finally selected for the experiments. With 0.50 mm nozzle diameters and a gap distance of 0.60 mm, a maximum apparent strain rate of 29 000 s^{-1} was achieved in the present equipment. Higher strain rates could be obtained by either decreasing the orifice entrances or by placing several pumps in parallel.[16] Using a smaller jet diameter ensured a stable flow field to the detriment of signal sensitivity following a reduction in the birefringence zone. With the second option, it was important that flow be kept well within the laminar regime.

Strain-Rate Calculation. Although the opposed-jets geometry has been thoroughly experimented during the last 2 decades,[1,10] the corresponding flow-field modelization is only available recently in the Newtonian limit.[17–19] In a narrow region along the symmetry axis, an approximate uniaxial extensional flow is created as fluid is pumped simultaneously into the nozzles. The fluid velocity starts from zero at the stagnation point, reaching v_0 at the orifice entrance. Assuming a uniform jet entrance velocity, an "apparent" fluid strain rate ($\dot{\epsilon}_{app}$) can be estimated from the relation:

$$\dot{\epsilon}_{app} = 2\bar{v}_0/L = 4Q/(\pi d^2 e) \quad (8)$$

where $\bar{v}_0$ is the volumetric average fluid velocity at the orifice, Q the total flow rate, d the jet diameter, and e the gap separating the two nozzles.

Most of the previous experiments in opposed-jets flow assumed uniform uniaxial extension in the region close to the central streamline. Recent flow simulations showed that this is not the case.[18] Changes in the local extensional strain rate can be as high as 100% over the region defined by the two jet entrances. Fortunately, the birefringence zone is highly localized along the centerline. The radial variation in strain rate over the effective zone probed by the laser beam is limited to <10%. The use of a locally averaged fluid strain rate which is a function only of the axial or flow direction (x) is, therefore, justified:

$$\dot{\epsilon}(x) = C(x)\, \dot{\epsilon}_{app} \quad (9)$$

The factor C depends on the exact flow geometry. Under the prevalent flow conditions, C has a value which increases continuously from 0.7 at the stagnation point to 0.9 near the orifice entrances.

To be consistent with previously published results, we will continue to use $\dot{\epsilon}_{app}$ in the present investigation. Since most of the reported data pertain to the stagnation point ($x = 0$),

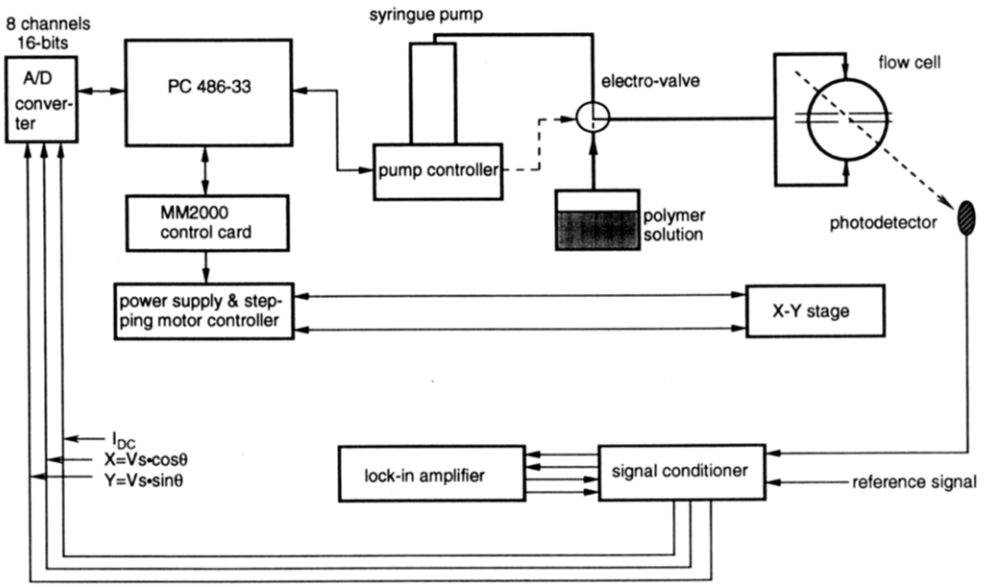

Figure 1. Schematic diagram of the flow birefringence system showing the major control and data acquisition components.

true values for $\dot{\epsilon}$ can be obtained after multiplying $\dot{\epsilon}_{app}$ by the correction factor 0.7.

Results and Discussion

Flow Birefringence Measurements. All the experiments have been conducted at room temperature (22 ± 0.5 °C).

The working principles of polarization-modulated optical rheometers have been reviewed by Fuller.[20] The configuration of the optical train to measure flow birefringence is depicted schematically in Figure 2. The intensity and polarization of the light beam can be calculated at any position along the optical train by multiplying the Stokes vector of the incident light with the appropriate Mueller matrices. By using that procedure, the output intensity at the detector position can be readily computed as:

$$I = (I_0/2)[1 + R_1 \sin(4\omega t) + R_2 \cos(4\omega t)] \quad (10)$$

where R_1 and R_2 are coefficients related to the retardation δ' and the orientation angle α of the birefringence zone with respect to the flow direction:

$$R_1 = -\cos(2\alpha) \sin(\delta') \quad (11a)$$

$$R_2 = \sin(2\alpha) \sin(\delta') \quad (11b)$$

Experimentally, the dc component $(I_0/2)$ is obtained from a low-pass filter which is part of the ROA signal conditioner. The coefficients R_1 and R_2 are detected with a dual-phase digital lock-in amplifier (Stanford Research Model 850). The orientation angle, α, is an important experimental parameter which depends on the local flow field. In a general situation like in simple shear flow[21] or in single-jet flow,[22] α is a function of the axial and radial positions. The situation is simpler in stagnant elongational flow with all the polymer chains oriented in the same direction at a constant angle α. The retardation δ' can thus be determined from a single evaluation of either R_1 or R_2.

One definite benefit of the polarization-modulation technique resides in the fact that the electric vector samples cyclically different projections of the refractive index tensor in the plane normal to the direction of light propagation. This feature renders possible real-time determination of δ' and α in a single experiment, in addition to the absolute values of δ' without any additional calibration (for example, δ' is negative for PS as a result of lateral orientation of the phenyl groups). Since the incident intensity is continuously monitored, fluctuations in the laser source are automatically cancelled out, resulting in an enhanced signal-to-noise ratio. Besides the gain in sensitivity, the polarization-modulation technique does not require dark-room facilities

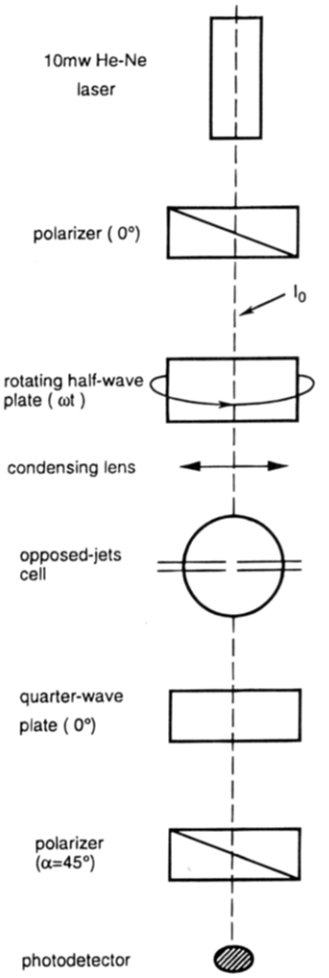

Figure 2. Diagram of the flow birefringence experiment showing the arrangement of optical elements.

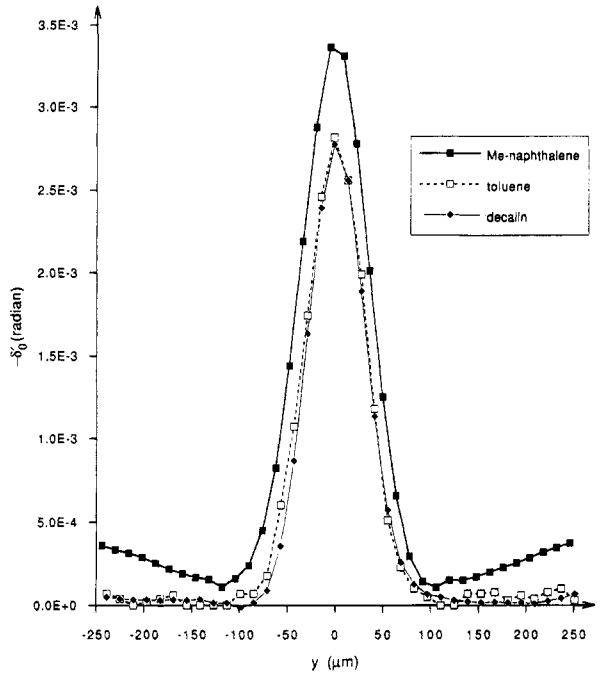

Figure 3. Retardation profiles for a 100 ppm PS solution (M_p = 6.85 × 10^6) recorded across the stagnation point in different solvents: (◆) in decalin at $\dot{\epsilon}_{app}$ = 25 500 s^{-1}; (□) in toluene at $\dot{\epsilon}_{app}$ = 25 500 s^{-1}; (■) in 1-methylnaphthalene at $\dot{\epsilon}_{app}$ = 17 000 s^{-1}.

which has hampered the widespread use of flow birefringence.

Flow Birefringence Profiles. The motorized X−Y stage (Micro-Contrôle MM2000) allowed raster scanning simultaneously with *"on the fly"*, data acquisition under the control of a PC-compatible computer. The "focal point" of the scanning beam was adjusted to coincide with the center of the flow. From diffraction theory, the focal region is approximately cylindrical with a "waist" given by:

$$d_f = 4\lambda f/\pi D \tag{12}$$

where λ = laser wavelength (632.8 nm), f = focal distance of the lens (63 mm), and D = diameter of the laser beam (0.8 mm at half-width).

The effective length, l_f, of the focal cylinder is approximatively given by:

$$l_f = 16\lambda f^2/\pi D^2 \tag{13}$$

By blocking and translating the laser light across a pinhole, a value of d_f = 0.06 mm was found for the diameter of the focused beam, in good agreement with the prediction of eq 12.

The axial retardation profiles, scanned along the direction y perpendicular to the flow direction, are given in Figure 3 for the three different solvents. The downward curvature of the baseline in 1-methylnaphthalene originates from the solvent birefringence which gives a positive retardation signal.

The birefringence, $\Delta n'$, is related to the retardation δ' by the relation:

$$\Delta n' = \delta'\lambda/(2\pi L) \tag{14}$$

(the same notation as given in the literature is used, i.e., a prime for birefringence and a double prime for dichroïsm[20]).

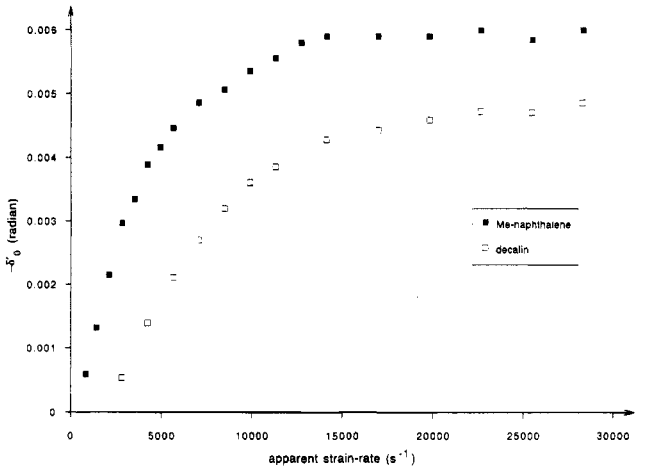

Figure 4. Maximum retardation (δ'_0) plotted as a function of $\dot{\epsilon}_{app}$ for a PS mixture (90 ppm M_p = 6.85 × 10^6 + 90 ppm M_p = 4.34 × 10^6): (□) in decalin; (■) in 1-methylnaphthalene.

In eq 14, λ is the laser wavelength (632.8 nm), and L, the thickness of the birefringence zone. Due to the inhomogeneous nature of the flow, the birefringence signal is not constant over the scanned volume but is an axisymmetric function of the radial distance r. Cathey and Fuller have shown that the birefringence $\Delta n'(r)$ can be recovered from the retardation profile, $\delta'(y)$, by the inverse Abel transformation.[23]

For *dilute* PS solutions, all the recorded transversal retardation profiles could be fitted to a Gaussian function of the form (Figure 3):

$$\delta'(y) = \delta_0' \exp(-y^2/2\sigma^2) \tag{15}$$

The maximum retardation δ_0' reached a plateau in the limit of high strain rates with a saturation value of −2.7 × 10^{-3} rad (or λ/2300) for a 100 ppm PS solution in decalin or in toluene and −3.3 × 10^{-3} rad in 1-methylnaphthalene (Figure 4).

When working with a low-viscosity solvent like toluene, some turbulence could be observed at flow rates Q > 50 mL/min ($\dot{\epsilon}_{app}$ > 6000 s^{-1}). In some instances where turbulences did not develop, a perfect Gaussian profile could be obtained even at the highest flow rate of 205 mL/min.

In a given solvent, the standard deviation σ of the retardation profile was found to be dependent on the strain rate and polymer MW. The effect, nevertheless, is weak and amounts to less than 10% in the dilute regime. The width of the retardation signal was similar in decalin and in toluene with σ equal to 27−30 μm (jets diameter 500 μm). This value increased in 1-methylnaphthalene to 33−37 μm. It should be remembered that the experimental σ contains a contribution from the width of the laser beam used to probe the retardation. Since l_f (~17 mm from eq 13) was much larger than the nozzle size, d_f could be taken as constant over the birefringence domain. The real standard deviation, σ^*, could then be estimated from the convolution relation of two Gaussian distribution functions:

$$\sigma^2 = \sigma^{*2} + \sigma_f^2 \tag{16}$$

where $\sigma_f \cong d_f/4$ is the standard deviation of the intensity distribution of the laser beam. The values of σ^* after correction were 23−26 μm in decalin or toluene and 30−34 μm in 1-methylnaphthalene.

The inverse Abel transform of a Gaussian function is also a Gaussian function of identical standard deviation:

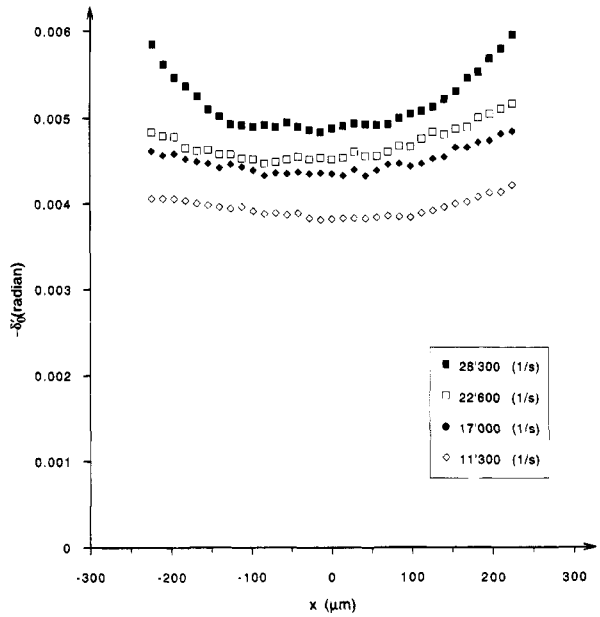

Figure 5. Maximum retardation δ'_0 for a PS mixture in decalin (90 ppm 6.85 × 10^6 M_p + 90 ppm 4.34 × 10^6 M_p) recorded along the flow direction, at different $\dot{\epsilon}_{app}$. The orifice entrances are respectively at $x = -300$ and 300 μm.

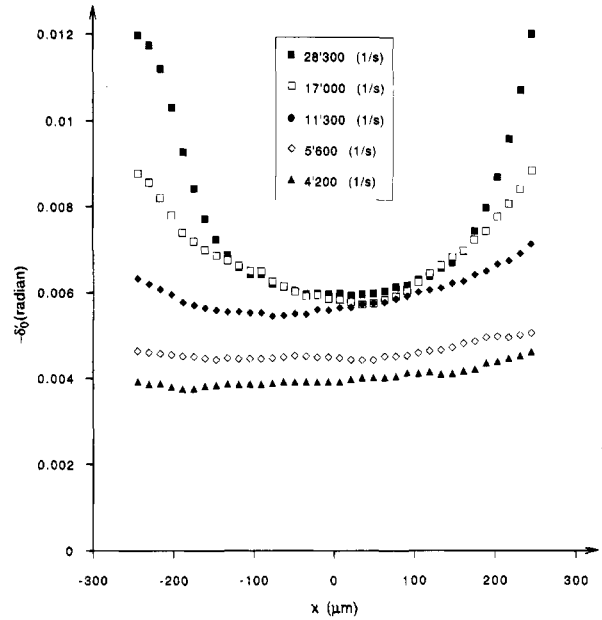

Figure 6. Maximum retardation δ'_0 for a PS mixture in 1-methylnaphthalene (90 ppm 6.85 × 10^6 M_p + 90 ppm 4.34 × 10^6 M_p) recorded along the flow direction, at different $\dot{\epsilon}_{app}$.

$$\Delta n'(r) = (2\pi)^{-1.5}\delta_0'(\lambda/\sigma)\exp(-r^2/2\sigma^2) \qquad (17)$$

Obviously, the difference in the width of the birefringence zone is reflected in the retardation signal. Since σ is 1.22 times larger in 1-methylnaphthalene than in decalin and toluene, the retardation signal should also be higher by the same factor in that solvent. This result has indeed been verified as is shown in Figure 4.

The maximum retardations, recorded at different positions along the symmetry axis, are given in Figures 5 and 6. Different behaviors were noted, depending on the values of $\dot{\epsilon}$. At low strain rates, $\delta_0'(x)$ was almost constant along the flow direction (x), indicating similar degrees of segmental orientation (Figure 5). At higher strain rates, an increase in the retardation signal was detected in the direction of the jets. This effect was particularly visible in 1-methylnaphthalene where the change in δ_0' reached almost 100% at $\dot{\epsilon}_{app} = 28\,300\ s^{-1}$ (Figures 6 and 7). The retardation profiles recorded near the orifices remained Gaussian with <15% increase in the standard width with respect to the value at the stagnation point (Figure 7). Since this variation was much smaller than the observed 2-fold change in the retardation signal, the phenomenon could only result from an increase in the intrinsic birefringence, i.e., from an increase in the degree of segmental orientation.

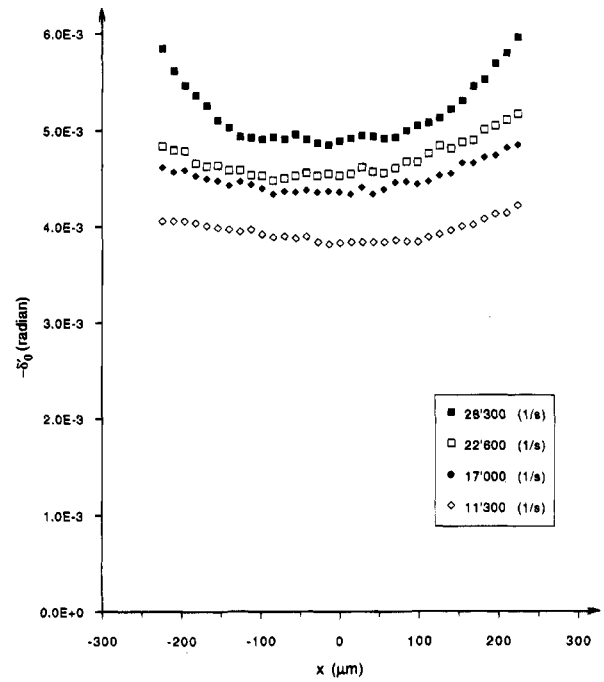

Figure 7. Retardation profiles for a 80 ppm PS solution in 1-methylnaphthalene recorded at different positions from the stagnation point ($M_p = 9.35 \times 10^6$, $\dot{\epsilon}_{app} = 14\,000\ s^{-1}$).

Polymer Concentration Dependence. Polymer concentration can influence the shape of the birefringence profile in a most dramatic way. With increasing polymer concentration and strain rate, the birefringence pattern changes from a narrow line to a "pipelike", structure and then finally to a delocalized zone with unstable boundaries ("flares"). This characteristic sequence of stages has been well-documented by Odell and Keller, who attributed this combined concentration/strain-rate dependence to the formation of a transient polymer network probed at different time scales ($\sim 1/\dot{\epsilon}$) for chain disentanglement.[24]

It is not the purpose here to study effects of polymer concentration. Rather, we wanted to determine the experimental conditions where intermolecular entanglements could be avoided. In Figure 8, the maximum retardation signal is shown as a function of strain rates for a 19 × 10^6 PS in decalin, at different polymer concentrations. Above a concentration of 100 ppm, δ_0' reached a maximum before leveling off to a lower plateau value. This maximum disappeared after cycling three times the polymer solution at $\dot{\epsilon}_{app} = 20\,000\ s^{-1}$. GPC analysis revealed a concomitant decrease in polymer MW as a result of flow-induced degradation. The retardation profile followed the previously mentioned pattern as a function of strain rate (Figure 9). The effect was even more pronounced in the good solvents toluene and 1-methylnaphthalene, where the typical pipelike structure with a central dark zone was fully developed at polymer concentrations as low as 100 ppm.

In order to avoid chain interactions, a polymer concentration of 60 ppm was used for experiments with

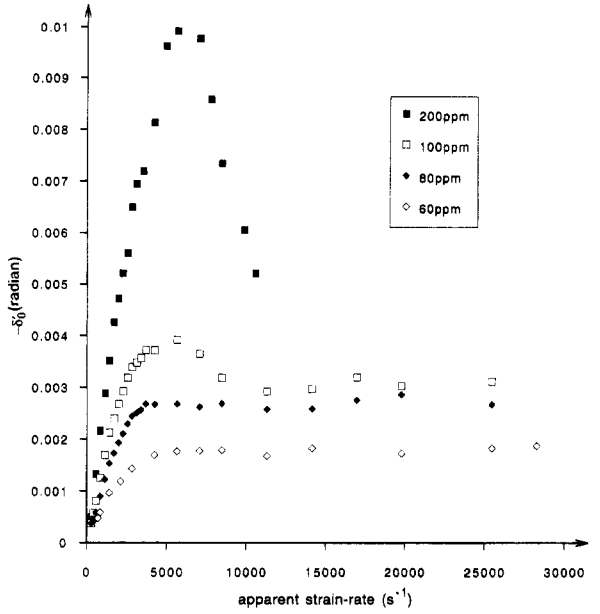

Figure 8. Maximum retardation (δ'_0) for a 19 × 10^6 PS solution in decalin plotted as a function of $\dot{\epsilon}_c$(app), at the indicated polymer concentrations.

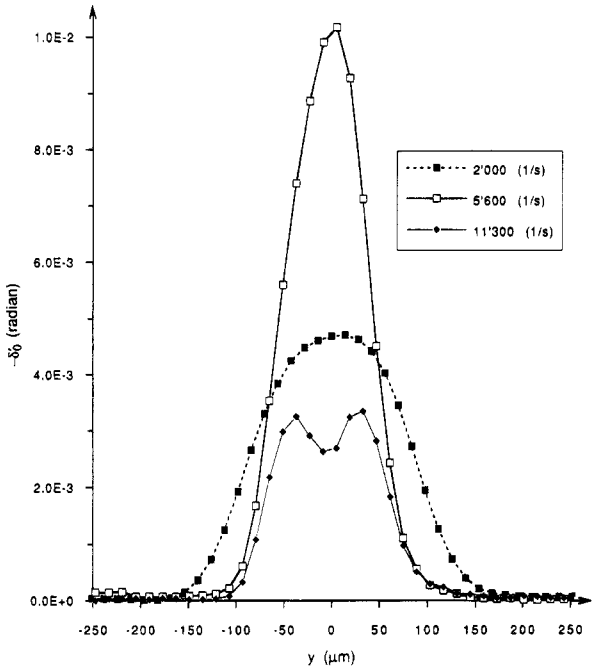

Figure 9. Effect of $\dot{\epsilon}_{app}$ on the retardation profile for a 200 ppm PS solution in decalin (M_p = 19 × 10^6).

ultrahigh-MW samples.

The molecular coil overlap concentration c^* under static conditions is given by the relation:[25]

$$c^* \cong 1.46/[\eta] \tag{18}$$

From the preceding results, it can be concluded that intermolecular interactions were already present in the vicinity of the stagnation point at polymer concentrations 2 orders of magnitude below c^*. The obtained value was almost 1 order of magnitude lower than the dynamic c^+ reported by the Bristol group for a 2.75 × 10^6 MW PS.[24] This low concentration limit put stringent requirements on the detection sensitivity which may be a source of uncertainty for equipment based on static polarization.

With the polarization-modulated instrument, it was possible to obtain reproducible retardation values at

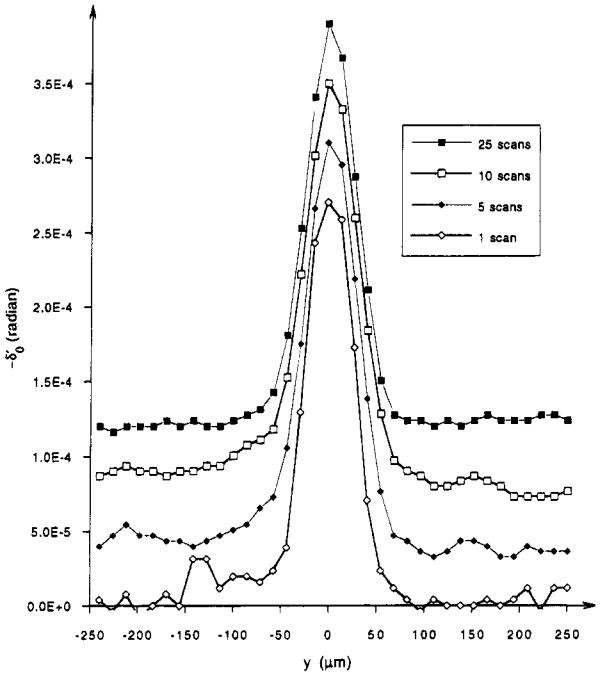

Figure 10. Retardation profile for a 10 ppm PS solution in decalin, showing the noise reduction effect of signal averaging (M_p = 19 × 10^6, $\dot{\epsilon}_{app}$ = 19 800 s^{-1}).

polymer concentrations below the 10 ppm level (Figure 10). Additionally, automatic data processing allowed suppression of spurious noise by signal averaging. The acquisition time, on the order of 2 s/scan, was mainly restricted by the stepping motor speed of 5000 $\mu m \cdot s^{-1}$. If time and solution volume were not the limiting factors, retardation at much lower concentrations could eventually be detected.

Molecular Weight Dependence. The retardation curve is a strong function of polymer MW. Since the critical strain rate for flow birefringence ($\dot{\epsilon}_c$) varies as the inverse of the chain relaxation time (eq 1), a dependence on $M^{-1.5}$ is expected in decalin.

The determination of this critical strain rate is, however, not without ambiguities. The problems associated with a precise determination of $\dot{\epsilon}_c$ are the following:

(a) The polymers used in the experiments were far from monodisperse. Even the best commercial standard with a polydispersity of 1.04 covers in practice a ~4-fold range of molecular weights, resulting in a spreading factor of $(4)^{1.5} = 8$ in $\dot{\epsilon}_c(M)$.

(b) The very existence of $\dot{\epsilon}_c$ is based on the assumption of an abrupt coil-to-stretch transition.[1] Recent simulation and experimental evidences tend to support a different picture, i.e., one in which submolecular orientation takes place before the occurrence of chain extension.[26-28] Progressive segmental orientation may further contribute to an additional broadening in the observed range of critical strain rates.

Most early studies identified $\dot{\epsilon}_c$ with the strain rate at the onset of flow birefringence.[10,29] From the preceding discussion, it is obvious that this quantity corresponds to the highest MW fraction present in solution and not to any of the molecular weight averages of the considered sample. In fact, the birefringence signal recorded at a given strain rate $\dot{\epsilon}_{M^*}$ resulted from the contribution of all polymer fractions with MW satisfying the condition given by eq 19:

$$M \geq M^* = [\dot{\epsilon}_{M^*}/A]^{1+a} \tag{19}$$

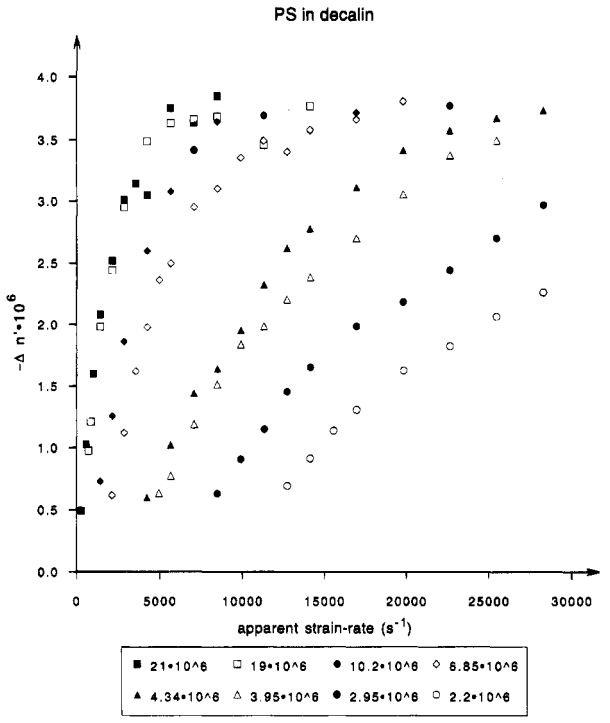

Figure 11. Maximum birefringence ($\Delta n'_0$) plotted as a function of $\dot{\epsilon}_c$(app) and polymer molecular weight, for dilute PS solutions in decalin (all the data are normalized to a polymer concentration of 100 ppm).

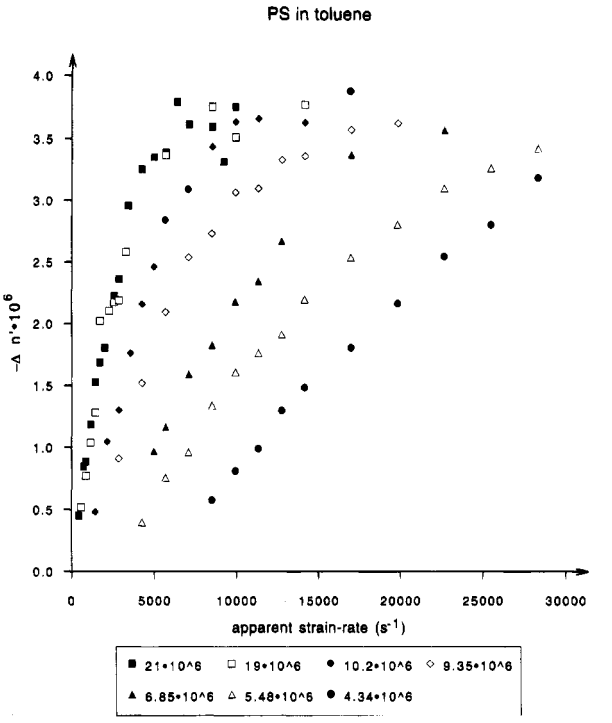

Figure 12. Maximum birefringence ($\Delta n'_0$) plotted as a function of $\dot{\epsilon}_{app}$ and polymer molecular weight, for dilute PS solutions in toluene (all the data are normalized to a polymer concentration of 100 ppm).

($\dot{\epsilon}_{M^*}$ is the critical strain rate for *monodisperse* polymer species with molecular weight M^*).

The corresponding retardation is therefore given by:

$$\delta'(\text{at } \dot{\epsilon}_{M^*}) = \alpha\int_{M^*}^{\infty} w_i(M)\,dM = \alpha\int_0^{\infty} w_i(M)\,dM - \alpha\int_0^{M^*} w_i(M)\,dM \quad (20)$$

All the birefringence curves determined in the dilute regime near the stagnation point reached the same limiting value at high strain rates for the three solvents of interest, i.e., $\Delta n'(0) = -3.8 \times 10^{-8}$/ppm (Figures 11–13). The literature data for the intrinsic birefringence of PS is -195×10^{-3}.[30] The corresponding $\Delta n'0$ calculated for the hypothetical case of fully oriented chains in solution is -18.4×10^{-8}/ppm. This value, which is by a factor of 5 larger than the saturation birefringence at the center of the jets, is still less than the observed value by a factor of ~2 near the orifice entrances in 1-methylnaphthalene.

From the preceding results, it can be concluded that the plateau region of the retardation curves *did not* correspond to a state of complete polymer extension. Although one may argue about the accuracy in the value used for intrinsic birefringence, the increase in $\Delta n'(0)$ toward the orifices strongly supports a model with progressive segmental orientation. Interestingly enough, an identical level of birefringence was reached near the stagnation point regardless of the solvent quality and polymer MW. From this constancy, eq 20 remains valid within a constant proportional factor:

$$\delta'_0(\text{plateau}) = \alpha\int_0^{\infty} w_i(M)\,dM \quad (21)$$

Equations 20 and 21 indicate a one-to-one correspondence between the birefringence curve and the integral molecular weight distribution $I(M)$ of the polymer sample:

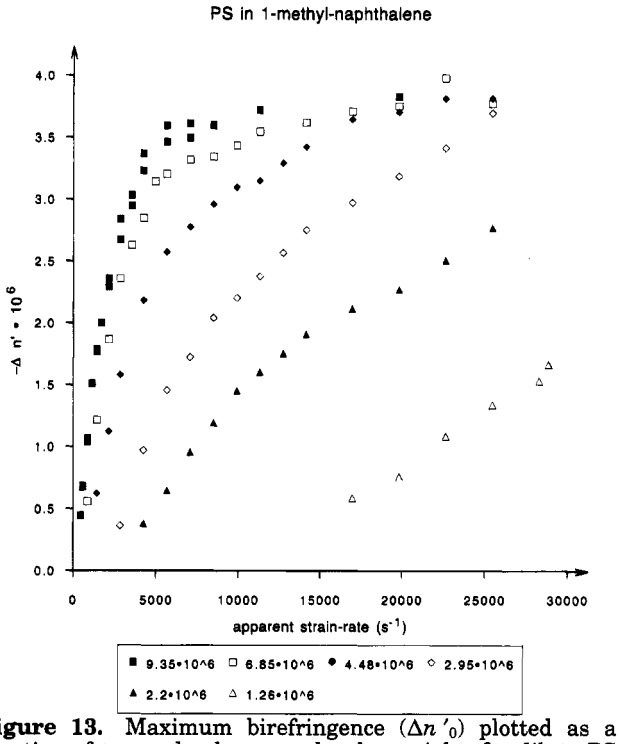

Figure 13. Maximum birefringence ($\Delta n'_0$) plotted as a function of $\dot{\epsilon}_{app}$ and polymer molecular weight, for dilute PS solutions in 1-methylnaphthalene (all the data are normalized to a polymer concentration of 100 ppm).

$$\delta'_0(\text{at } \dot{\epsilon}_{M^*})\delta'_0(\text{plateau}) = 1 - \int_0^{M^*} w_i(M')\,dM' = 1 - I(M^*) \quad (22)$$

Fitting the birefringence curve to the integral MWD would be the most correct way to derive $\dot{\epsilon}_c(M)$.[16] Precise determination of MWD in the ultrahigh-MW range is, however, a time-consuming enterprise requiring extensive calibrations and data manipulations to correct for instrumental spreading.[15,16] To circumvent some of

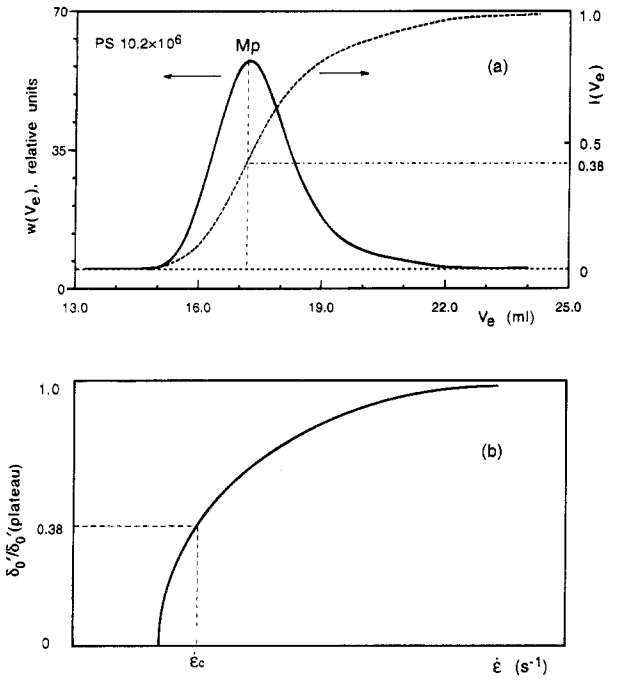

Figure 14. Experimental determination of the critical strain rate ($\dot{\epsilon}_c$(app)) for flow birefringence: (a) differential and integral MWD for a 10.2 × 10^6 PS standard; (b) normalized retardation curve and the determination of $\dot{\epsilon}_c(M_p)$.

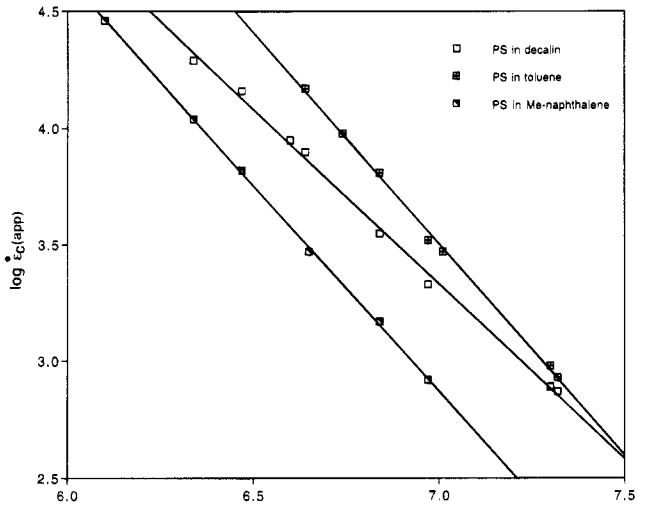

Figure 15. Double-logarithmic plot of the dependence of $\dot{\epsilon}_c$(app) on polymer molecular weight for dilute PS solutions in decalin, toluene, and 1-methylnaphthalene.

these problems, we used a graphical technique based on the molecular weight at peak maximum (M_p) to determine the corresponding critical strain rate $\dot{\epsilon}_c(M_p)$. The procedure, illustrated in Figure 14, consisted of localizing the peak maximum from the GPC trace and then calculating the value corresponding to δ'_0(plateau) $[1 - I(M_p)]$ on the birefringence curve.

The experimentally determined critical strain rates $\dot{\epsilon}_c(M_p)$ in decalin are plotted in Figure 15 as a function of M_p on a double-logarithmic scale. A good straight line with a slope of -1.5 ± 0.02 was obtained which confirms the theoretical prediction of eq 1 in a poor solvent.

For a given polymer MW, chains are more expanded in a good solvent than in a poor solvent. This additional swelling of the molecular coils reduces the entropic restoring forces and favors the gripping action of the solvent molecules during "strong" flow deformation. From this reasoning, it is expected that molecular coils are more readily deformed in a good solvent than in a poor solvent. Previous flow birefringence investigations failed to detect such a solvent effect. This negative result was explained by a nonuniform stretching of the molecular coils which remain curled near the chain ends.[12]

In the present investigation, toluene and 1-methylnaphthalene were selected as good solvents for PS. Decalin has almost the same viscosity as 1-methylnaphthalene; thus, any difference in the birefringence curves in these two solvents could be ascribed mainly to the effect of solvation.

By using the previous technique for determining $\dot{\epsilon}_c(M_p)$, straight lines were obtained on a log–log plot of the critical strain rates as a function of MW (Figure 15). The slopes of -1.8 ± 0.04 for toluene and -1.77 ± 0.03 for 1-methylnaphthalene are in fair agreement with eq 1 but are in contradiction with results reported in the literature. The reason for this discrepancy may be partly traced back to the different procedures used in the estimation of $\dot{\epsilon}_c(M)$.

Determination of the Proportionality Factor B. The longest intramolecular relaxation time, τ_1, is certainly the single most important parameter in any description of polymer chain dynamics. Predicted respectively by Rouse[31] and Zimm[32] in the limits of free-draining and non-free-draining chains, τ_1 (eq 2) can be conveniently expressed in the form:

$$\tau_1 = \eta_s[\eta]M/(A_1RT) \tag{23}$$

The numerical factor A_1 is 0.822 for the free draining chain,[31] 1.184 for the non-free-draining chain with preaveraged hydrodynamic interactions,[32] and 0.574 without preaveraging the Oseen tensor.[33]

Since there is some controversy on the correct value for A_1, we will base our discussion on experimentally determined quantities. Dynamic light scattering is a unique technique for probing internal motions of a flexible polymer in solution. From the spectrum of scatttered light, different methods of analysis have been applied to estimate τ_1 for comparison with the theoretical predictions.[34–37] In some studies, it has been found that PS at infinite dilution, either in good (benzene) or poor (*trans*-decalin) solvents, behaves according to the Zimm model with $A_1 \cong 1.2$.[34,35] Recent investigations[36,37] have confirmed the value of 1.2 in poor solvents. In ethylbenzene, a good solvent for PS, a smaller value of $A_1 = 0.84$ has been obtained. This latter result is qualitatively consistent with an increasing draining effect with the more expanded coils.

Using $A_1 = 1.2$ for decalin and 0.84 for toluene and 1-methylnaphthalene, the following numerical expressions have been derived for τ_1:

$$\tau_1\,(\text{decalin}) = 1.90 \times 10^{-9} M^{1.53}\,(\text{s}) \tag{24}$$

$$\tau_1\,(\text{toluene}) = 4.48 \times 10^{-10} M^{1.71}\,(\text{s}) \tag{25}$$

$$\tau_1\,(\text{1-methylnaphthalene}) = 2.74 \times 10^{-9} M^{1.70}\,(\text{s}) \tag{26}$$

(exceptionally, M is expressed here in units of kg·mol^{-1}).

To obtain the proportionality factor B in eq 1, $\dot{\epsilon}_c$(app) is first converted into $\dot{\epsilon}_c$ by applying the correction factor 0.7 (eq 9). The product $\dot{\epsilon}_c\tau_1 \equiv B$ is then calculated for the different polymer solutions. Within experimental errors, B is independent from the polymer MW but

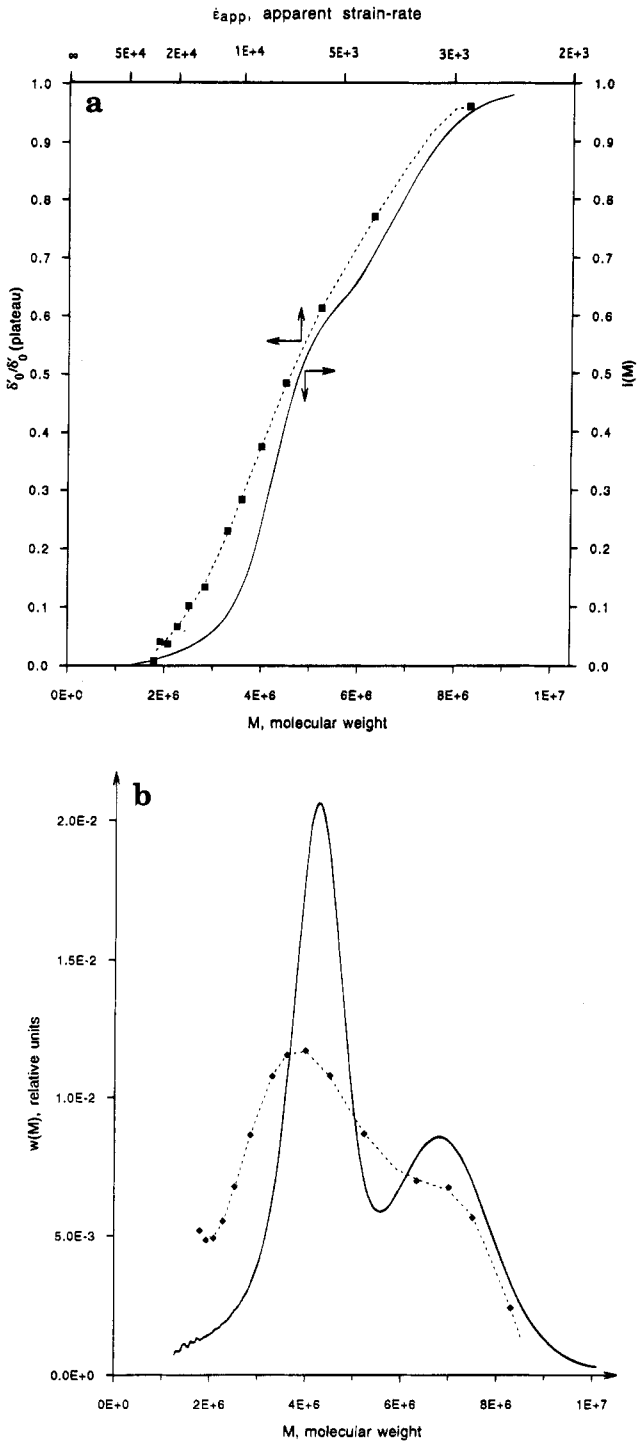

Figure 16. Comparison between the MWD determined by gel permeation chromatography (—) and calculated from the retardation curve (- - -) for a PS mixture (90 ppm $M_p = 6.85 \times 10^6$ + 90 ppm $M_p = 4.34 \times 10^6$): (a) integral MWD; (b) differential MWD. (Experimental conditions for GPC analysis: columns 2 × TSK G7000 HXL + 1 × Ultrastyragel 10^6 Å; eluent THF at 0.300 mL/min.)

changes with the nature of the solvent. From 3 in decalin, B increases to 6 in toluene and finally to 8 in 1-methylnaphthalene. In any case, the obtained values are significantly larger than the theoretical estimates of 0.5–1 cited in the Introduction.

Several explanations may be proposed to account for the large experimental values for B:

(1) Incorrect assignment of the local strain rate ($\dot{\epsilon}$). As mentioned in the Experimental Section, a Newtonian fluid was used for flow-field modelization. It is known that the velocity gradient may be significantly perturbed by the presence of polymer molecules even at very low concentrations.[38] The coupling between the macroscopic flow field and the molecular deformation may sufficiently alter the local flow field to invalidate the use of eqs 8 and 9 in the calculation of $\dot{\epsilon}$. The fact that the birefringence curves for the two most dilute solutions (80 and 60 ppm in Figure 8) are superposable after normalization to the same polymer concentration is a strong indication that non-Newtonian effects are negligible below 100 ppm under the present experimental conditions.

(2) Incomplete account of the chain dynamics with a single molecular relaxation time. The Rouse and Zimm relaxation times are derived under the condition of minute deformation of the molecular coils.[7] Alternative models like the "prestretched",[12] the "yo-yo",[39] or the "kinked"[40] chain used to describe larger chain extension may require different relaxation times.

(3) Complications due to form birefringence.[41] The effect should be absent in 1-methylnaphthalene as a result of the refractive index matching between polystyrene (n_D^{20} = 1.59–1.60) and the solvent (n_D^{20} = 1.614). Since form birefringence is always positive, whereas intrinsic birefringence is negative for PS, we have attempted to detect changes in the retardation sign in toluene and decalin at low strain rate (n_D^{20}(decalin) = 1.474, n_D20(toluene) = 1.497). No such effect was observed: it is concluded that form birefringence is negligible under elongational flow conditions.

(4) Progressive increase of the birefringence signal with $\dot{\epsilon}$, even for a monodisperse polymer fraction. The fact that B is greater in toluene and in 1-methylnaphthalene than in decalin seems to indicate a more gradual segmental orientation in good solvents. From this picture, one may argue that extrapolating $\dot{\epsilon}_c$ to the limit of zero birefringence would be the better choice. This procedure, however, is sensitive to the sample polydispersity. In addition, $\dot{\epsilon}_c$ loses its physical meaning if a sudden coil-to-stretch transition is not fulfilled.

Whether the birefringence signal shows an abrupt transition or increase monotonically with the fluid strain rate is an important test of the different models of chain uncoiling. The large dispersion of the experimental birefringence curves (cf. section below) seems to favor the latter explanation and will be detailed in a coming publication.[16]

Molecular Weight Distribution from Flow Birefringence. Flow birefringence has been proposed as a potential technique for MWD characterization.[9] To verify this feasibilty, we have recorded the retardation curve for a 1:1 mixture of two PS standards differing in M_p by a factor 1.6 (Figure 4). The transformation of the retardation curve into the MWD was accomplished in two steps, using the following procedure. First, the retardation signal $\delta'_0(\dot{\epsilon})$ was converted into $I(M)$ (Figure 16a), using eq 22 and the scaling law obtained from the data of Figure 13 for PS/decalin:

$$\log \dot{\epsilon}_c(\text{app}) = 13.617 - 1.5013 \log M \quad (27a)$$

$$M = 1.18 \times 10^9 \dot{\epsilon}_c(\text{app})^{-0.666} \quad (27b)$$

The differential MWD was then calculated from the derivative of $I(M)$ after fitting the data to a seventh-order polynomial to reduce spurious noise. The final results are given in Figure 16b along with the GPC data. Even without instrumental broadening correction, the GPC chromatogram distinctly revealed the bimodal distribution. Flow birefringence, on the other hand, was incapable of resolving clearly the two components of the

blend. The large spread in the flow birefringence curve may stem from a progressive segmental orientation with increasing flow rate, an effect which has been suggested in the previous section. More details about the spreading function could, in principle, be obtained from a careful comparison between the GPC data and the retardation curves.

From the present study, one can conclude that the resolution of flow birefringence is well below the separation capability of GPC, even in the highest MW range where axial dispersion is important with the latter technique. Moreover, flow birefringence suffers from two additional disadvantages which make the method less attractive than conventional GPC:

(1) The computation of M from $\dot{e}$ involves a nonlinear transformation. Data points are unevenly distributed along the MW scale, resulting in a degraded performance in the high-MW region.

(2) Differentiation is required to recover the MWD from the retardation curve. Differentiation exacerbates the effects of noise, making the whole procedure sensitive to extraneous sources of disturbance.

Conclusion

In this paper, we have evaluated the advantages of using a polarization-modulated optical rheometer for the studies of flow birefringence. The gain in sensitivity was significant and, according to experiments performed under identical conditions, is a factor of 5–8 better than the classical (static) polarimeters. This may seem a modest improvement in view of the additional instrumentational complexity. It is, however, crucial for a successful investigation of single molecular chain dynamics in which highly dilute polymer solutions are required. The stability of the birefringence signal allowed multiple scanning, and some additional improvement in the signal-to-noise ratio could be achieved over reasonable times by signal averaging. The increased speed of operation of the instrument permitted more data to be collected in a given time, thus improving the overall reliability of the measurements. Efficient use of a given volume of polymer solution was a definite asset in some experiments, such as in transient elongational flow, where high mechanochemical degradation precludes the recirculation of the polymer solution.[22,42]

With the instrument described, we have been able to determine the influence of solvent quality on the birefringence signal. The width of the retardation curve for a broadly distributed polymer sample seemed to indicate a progressive segmental orientation in flow. Under such conditions, the critical strain rate loses its physical meaning, and the scaling laws which relate $\dot{\epsilon}_c$ to MW as well as the coil-to-stretch transition model need to be reconsidered.

Acknowledgment. Assistance of G. G. Fuller (Stanford University) during the initial setup of the ROA instrument and D. J. Hunkeler (Vanderbilt University) for light scattering measurements is highly appreciated. T.Q.N. greatly benefitted from helpful discussions with J. Odell, P. Pincus, and Y. Rabin during the preparation of this manuscript. Financial support from the Swiss National Science Foundation is gratefully acknowledged.

References and Notes

(1) Pope, D. P.; Keller, A. *Colloid Polym. Sci.* **1978**, *256*, 751.
(2) De Gennes, P.-G. *J. Chem. Phys.* **1974**, *60*, 5030.
(3) Tanner, R. I. *Engineering Rheology*, revised ed.; Clarendon Press: Oxford, U.K., 1988; pp 184–190.
(4) Magda, J. J.; Larson, R. G.; Mackay, M. E. *J. Chem. Phys.* **1988**, *89*, 2504.
(5) Larson, R. G.; Magda, J. J. *Macromolecules* **1989**, *22*, 3004.
(6) Mueller, A. J. Extensional Flow of Macromolecules in Solution Ph.D. Dissertation, University of Bristol, 1989; p 20.
(7) Doi, M.; Edwards, S. F. *The Theory of Polymer Dynamics*; Clarendon Press: Oxford, U.K., 1986; pp 100–114.
(8) Ohta, T.; Oono, Y.; Freed, K. F. *Phys. Rev. A* **1982**, *25*, 2801.
(9) Farrell, C. J.; Keller, A.; Miles, M. J.; Pope, D. P. *Polymer* **1980**, *21*, 1292.
(10) Keller, A.; Odell, J. A. *Colloid Polym. Sci.* **1985**, *263*, 181.
(11) Rabin, Y.; Henyey, F. S.; Pathria, R. K. *Phys. Rev. Lett.* **1985**, *55*, 201.
(12) Rabin, Y. *J. Chem. Phys.* **1988**, *88*, 4014.
(13) Fuller, G. G.; Mikkelsen, K. J. *J. Rheol.* **1989**, *33*, 761.
(14) Nguyen, T. Q.; Kausch, H. H. *Macromolecules* **1990**, *23*, 5137.
(15) Nguyen, T. Q.; Kausch, H. H. Proceedings of the International GPC Symposium '91, San Francisco, CA, Oct 13–16, 1991.
(16) Nguyen, T. Q.; Yu, G.; Kausch, H. H., to be submitted to *Colloid Polym. Sci.*
(17) Schunk, P. R.; de Santos, J. M.; Macosko, C. W.; Scriven, L. E. Proceedings of the Xth International Congress on Rheology, Sydney, Australia, 1988, *Vol. 2*, p 254.
(18) Tatham, J. P. Extensional Flow Dynamics of Macromolecules of Differing Flexibility in Solution. Ph.D. Dissertation, University of Bristol, 1993, pp 91–110.
(19) Tatham, J. P.; Carrington, S. C.; Sáez, E. A.; Odell, J. A., to be published in *Polymer*.
(20) Fuller, G. G. *Annu. Rev. Fluid Mech.* **1990**, *22*, 387.
(21) Chow, A. W.; Fuller, G. G. *J. Rheol.* **1984**, *28*, 23.
(22) Nguyen, T. Q.; Kausch, H. H. *Adv. Polym. Sci.* **1992**, *100*, 73.
(23) Cathey, C. A.; Fuller, G. G. *J. Non-Newtonian Fluid Mech.* **1990**, *34*, 63.
(24) Chow, A.; Keller, A.; Müller, A. J.; Odell, J. A. *Macromolecules* **1988**, *21*, 250.
(25) Fujita, H. *Polymer Solutions*, *Studies in Polymer Science 9*; Elsevier: New York, 1990; p 179.
(26) Wiest, J. M.; Wedgewood, L. E.; Bird, R. B., *J. Chem. Phys.* **1989**, *90*, 587.
(27) Hunkeler, D.; Nguyen, T. Q.; Kausch, H. H. *Polym. Prepr. (Am. Chem. Soc., Div. Polym. Chem.)* **1991**, *32* (2), 667.
(28) Liu, T. W. *J. Chem. Phys.* **1989**, *90*, 5827.
(29) Brestkin, Y. V.; Saddikov, I. S.; Agranova, S. A.; Baranov, V. G.; Frenkel, S. *Polym. Bull.* **1986**, *15*, 147.
(30) Seferis, J. C. *Polymer Handbook*, 3rd ed.; Brandrup, J., Immergut, E. H., Eds.; John Wiley & Sons: New York, Toronto, 1989; pp VI-451.
(31) Rouse, P. E. *J. Chem. Phys.* **1953**, *21*, 1272.
(32) Zimm, B. H. *J. Chem. Phys.* **1956**, *24*, 269.
(33) Bixon, M.; Zwanzig, R. *J. Chem. Phys.* **1978**, *68*, 1890.
(34) Tsunashima, Y.; Nemoto, N.; Kurata, M. *Macromolecules* **1983**, *16*, 584.
(35) Nemoto, N.; Makita, Y.; Tsunashima, Y.; Kurata, M. *Macromolecules* **1984**, *17*, 425.
(36) Bhatt, M.; Jamieson, A. M. *Macromolecules* **1989**, *22*, 2724.
(37) Nicolai, T.; Brown, W.; Johnsen, R. *Macromolecules* **1989**, *22*, 2795.
(38) Leal, L. G. In Proceedings of the 1985 La Jolla Institute Workshop. *Polymer-Flow Interaction*; Rabin, Y., Ed.; Academic International Press, New York, 1986; p 5.
(39) Ryskin, G. *J. Fluid Mech.* **1987**, *178*, 423.
(40) Larson, R. G. *Rheol. Acta* **1990**, *29*, 371.
(41) Tsetkov, V. N. *Vyskomol. Soedin. (Engl. Transl.)* **1963**, *5*, 1448, 1456.
(42) Nguyen, T. Q.; Kausch, H. H. *J. Non-Newt.Fluid Mech.* **1988**, *30*, 125.

MA9462969